Journal of Alloys and Compounds 509 (2011) 7143–7151

Contents lists available at ScienceDirect

Journal of Alloys and Compounds

journal homepage: www.elsevier.com/locate/jallcom

The effects of graphite on the reversible hydrogen storage of nanostructured lithium amide and lithium hydride ($LiNH_2 + 1.2LiH$) system

R.A. Varin*, M. Jang

Department of Mechanical and Mechatronics Engineering, University of Waterloo, Waterloo, Ontario, Canada, N2L 3G1

ARTICLE INFO

Article history:
Received 7 March 2011
Accepted 5 April 2011
Available online 12 April 2011

Keywords:
Hydrogen storage
Hydrides
Lithium amide/imide
Ball milling
Graphite additive

ABSTRACT

The addition of 5 wt.% of graphite was incorporated into the ($LiNH_2 + 1.2LiH$) hydride system in order to study its effect on the prevention of LiH from hydrolysis/oxidation which leads to the escape of NH_3. The composite hydride system was processed by ball milling for 25 h. Thermal behavior in DSC up to 500 °C and isothermal desorption in a Sieverts-type apparatus were carried out. XRD was used to obtain information about phase changes. It is found that after ball milling graphite becomes amorphous. DSC analysis shows that for the mixture (($LiNH_2 + 1.2LiH$) + 5 wt.% graphite) graphite can prevent or at least substantially reduce the oxidation/hydrolysis of LiH since no melting peak of retained $LiNH_2$ is observed. Both the DSC and Sieverts-type tests show that the addition of graphite increases the apparent activation energy of desorption from the ~57–58 to ~85–90 kJ/mol range. On the other hand, the graphite additive increases measurably the desorbed/absorbed capacity of hydrogen at 275, 300 and 325 °C. The (($LiNH_2 + 1.2LiH$) + 5 wt.% graphite) system is fully reversible desorbing/absorbing ~5 wt.% H_2 at 325 °C in the following reaction: ($LiNH_2 + LiH \leftrightarrow Li_2NH + H_2$). Step-wise pressure–composition–temperature (PCT) tests show that the enthalpy and entropy change of this reversible reaction is −62.4 and −61.0 kJ/mol H_2 and 117.8 and 115.8 J/mol K for undoped and 5 wt.% G doped ($LiNH_2 + 1.2LiH$) system, respectively. It shows that within an experimental error there is no measurable effect of graphite additive on the thermodynamic properties. The Van't Hoff analysis of the obtained thermodynamic data shows that the equilibrium temperature at atmospheric pressure of hydrogen (1 bar H_2) is 256.8 and 253.9 °C for the undoped and 5 wt.% G doped ($LiNH_2 + 1.2$ LiH) system ball milled for 25 h, respectively. Such high equilibrium temperatures render it rather obvious that both of these hydride systems cannot be employed for hydrogen desorption/absorption below 100 °C as required by the DOE targets for the automotive hydrogen storage materials.

1. Introduction

Hydrogen is perceived as a future energy carrier that may gradually allow the transformation from the fossil fuel based economy to the hydrogen economy. However, a widespread hydrogen use particularly for transportation/automotive applications is hindered by three major obstacles: (a) improvement of fuel cells which produce electrical current and water vapor when fuelled by hydrogen, (b) inexpensive hydrogen production and (c) hydrogen storage [1]. The latter obstacle is most likely the most important one, particularly for automotive applications. Since for various reasons gaseous and liquid hydrogen storage techniques are very cumbersome to commercialize [1] a general consensus emerged that the only remaining option is solid state hydrogen storage in hydrides.

One group of hydrides that have attracted attention for practical storage is based on lithium-nitrogen-based hydrides (lithium amide $LiNH_2$ and imide Li_2NH). The available papers on the hydrogen storage behavior of this group of hydrides published until the end of 2008 have been reviewed in [1]. Chen et al. [2] were the first researchers to report the following reversible reaction in the Li–N–H (lithium amide–lithium hydride–lithium imide) system

$$LiNH_2 + LiH \leftrightarrow Li_2NH + H_2 \quad (1)$$

Reaction (1) can desorb and re-absorb a relatively large theoretical amount of 6.5 wt.% hydrogen. Chen et al. calculated the enthalpy change (ΔH) of this reaction as being equal to about −45 kJ/mol. However, it has been recently claimed that the enthalpy change was closer to about −66 kJ/mol [3], which seems to be less favorable for practical applications since according to the Van't Hoff rule [1] it results in a higher equilibrium temperature under 1 bar H_2 pressure. Another problem with reaction (1) is that it releases ammonia (NH_3) during desorption [1] which can be poisonous for the membrane of a conventional proton exchange membrane (PEM) fuel cell,

* Corresponding author. Tel.: +1 519 888 4567; fax: +1 519 885 5862.
E-mail addresses: ravarin@uwaterloo.ca, ravarin@mecheng1.uwaterloo.ca (R.A. Varin).

0925-8388/$ – see front matter © 2011 Elsevier B.V. All rights reserved.
doi:10.1016/j.jallcom.2011.04.036

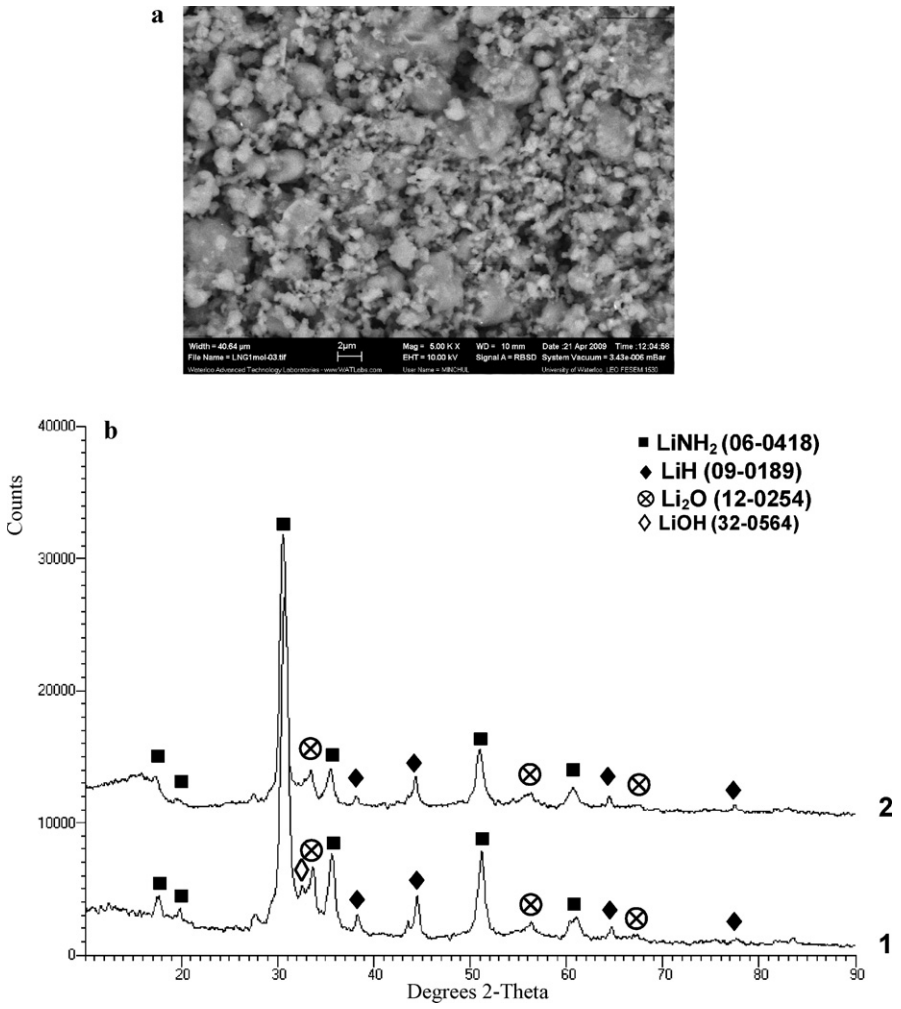

Fig. 1. (a) Backscattered electrons (BSE) micrograph of (($LiNH_2$ + 1.2LiH) + 5 wt.% G) and (b) XRD patterns for 1-(($LiNH_2$ + 1.2LiH) and 2-(($LiNH_2$ + 1.2LiH) + 5 wt.% G) both milled for 25 h.

even at trace levels so at present even a relatively small release of ammonia in the hydrogen gas cannot be tolerated in the system.

It has been rather well documented [1,4–9] that reaction (1) proceeds with two intermediate elementary reactions (2) and (3):

$$2LiNH_2 \rightarrow Li_2NH + NH_3 \quad (2)$$

$$NH_3 + LiH \rightarrow LiNH_2 + H_2 \quad (3)$$

with the enthalpy change of +84 kJ/mol NH_3 and −42 kJ/mol H_2, respectively.

In these reactions $LiNH_2$ (lithium amide) decomposes into Li_2NH (lithium imide) and NH_3, and then the emitted NH_3 reacts extremely fast (in microseconds [9,10]) in reaction (3) with LiH to form $LiNH_2$ and H_2. The newly formed $LiNH_2$ decomposes again and repeats the cycle of reactions (2) and (3). Such successive reactions continue until all $LiNH_2$ and LiH completely transform to Li_2NH and H_2. Recently, Shaw et al. [9] reported that high energy ball milling of the $LiNH_2$ + 1.1LiH system, where the 10% excess of LiH was added to minimize the loss of NH_3 during dehydrogenation, resulted in the near elimination of the escaping NH_3 at a heating rate of 5 °C/min and the 60% reduction in the apparent activation energy of reaction (1). Nevertheless, despite such a fast rate of reaction (3) in ball milled mixture the escape of NH_3 is still observed. Ikeda et al. [11] reported that the hydrogen capacity of the ball milled ($LiNH_2$ + 1.1LiH) system decayed substantially during 200 cycles at 300 °C due to the nitrogen loss due to escaping NH_3.

Most recently, we have reported [12] that the major problem with escaping NH_3 is the oxidation/hydrolysis of LiH in the ($LiNH_2$ + LiH) system. We have shown that the unreacted/retained $LiNH_2$ will always release NH_3 as long as a part of LiH becomes inactive due to the hydrolysis/oxidation and does not take part in the intermediate reactions (2) and (3). To solve these problems, LiH should be prevented from oxidation and hydrolysis. Also, we have shown that the ($LiNH_2$ + 1.2LiH) molar ratio in the mixture ball milled for 25 h results in the lowest apparent activation energy of dehydrogenation of reaction (1) being equal to ∼58 kJ/mol which is even lower than the one reported by Shaw et al. [9] for the 1:1.1 molar ratio (∼63 kJ/mol).

The present work is the continuation of our research on the hydrogen storage properties of ball milled ($LiNH_2$ + 1.2LiH) mixture as reported in [12]. In the present work we added 5 wt.% of graphite to assess how it prevents LiH from oxidation/hydrolysis and as such mitigates the NH_3 escape. We anticipate that graphite after ball milling would be relatively evenly distributed as a thin coat around LiH particles. That could seal off the LiH particles from the effects of the environment/moisture. The amount of 5 wt.% of graphite (G) was added to the mixture with the molar ratio ($LiNH_2$ + 1.2LiH) which was processed by ball milling for 25 h. The ball milled powders were subsequently investigated by scanning electron microscopy (SEM), differential scanning calorimetry (DSC), X-ray diffraction (XRD) and volumetric hydrogen desorption/absorption in a Sieverts-type apparatus.

2. Experimental

$LiNH_2$ (purity 95%), LiH (purity 95%) and a synthetic graphite (G) powder (particle size <20 μm) were purchased from Sigma–Aldrich. The mixtures were prepared with the following molar and weight ratios: ($LiNH_2$ + 1.2LiH) and (($LiNH_2$ + 1.2LiH) + 5 wt.% G). Subsequently, they were processed by mechanical milling for 25 h in order to achieve nanostructuring [12]. The selected milling mode in the magneto-mill, Uni-Ball-Mill 5 (A.O.C. Scientific Engineering Pty Ltd., Australia) [1,13–15], was high-energy impact (IMP68 with magnets at 6 and 8 o'clock position) at 225 rpm using four steel balls (see Fig. 1 in [12]). The ball-to-powder weight ratio (R) was 40:1 (R40). The pressure of high purity hydrogen (purity 99.999%: O_2 < 2 ppm; H_2O < 3 ppm; CO_2 < 1 ppm; N_2 < 6 ppm; CO < 1 ppm; THC < 1 ppm) in the vial was always kept constant at ~600 kPa during the entire milling process. Through the entire milling process the milling vial was continuously cooled with an air fan. All the powder handlings before and after milling were performed in a purged glove box under overpressure of high purity argon (purity 99.999%) in order to minimize any possible contamination by moisture or oxygen from air. The images of ball milled powders were obtained using a high-resolution, field emission SEM (FE SEM) LEO 1530 using backscattered electrons (BSE) mode.

The crystal structure of powders was characterized with a Bruker D8 X-ray diffractometer. Monochromated Cu $K\alpha_1$ radiation was used. An accelerating voltage of 40 kV and a current of 30 mA were used. The scan range was from $2\theta = 10^\circ$ to 90° at the rate of $3^\circ\,min^{-1}$ with a step size of 0.05°. A home-made environmental brass holder with a Cu/glass plate for powder support was loaded in a glove box filled with high purity Ar. Upper and lower part of the environmental holder is sealed through a soft-rubber O-ring and tightened using threaded steel bolts with nuts.

The thermal behavior of freshly ball milled powders was studied by differential scanning calorimetry (DSC) (Netzsch 404) of ~5 mg samples in an alumina crucible. Samples were heated to 500 °C at a heating rate of 2, 5, 10 and 15 °C/min and argon flow rate of 100 ml/min in order to estimate the activation energy by using the Kissinger equation [1]:

$$\frac{d\,\ln(\beta/T_p^2)}{d(1/T_p)} = -\frac{E_A}{R} \tag{4}$$

where β is the heating rate, T_p the peak temperature, E_A the activation energy, and R is the gas constant.

The hydrogen desorption/absorption was evaluated using a second generation volumetric Sieverts-type apparatus custom-built by A.O.C. Scientific Engineering Pty Ltd., Australia. This apparatus built entirely of austenitic stainless steel allows loading of a powder sample in a glove box under argon and its subsequent transfer to the main unit in a sealed austenitic stainless steel sample reactor without any exposure to the environment. The weight of the powder sample in the desorption experiments was in the range of 2–30 mg. The calibrated accuracy of desorbed hydrogen capacity is about ±0.1 wt.% H_2 and that of temperature reading ±0.1 °C. Before starting the desorption test, the inner tubing of the apparatus and reactor were evacuated and purged 4 times with argon and then two times with hydrogen. The furnace of the apparatus was heated separately to the desired test temperature and subsequently inserted onto a tightly sealed powder sample reactor inside which an atmospheric pressure of 1 bar H_2 was kept. Hence, the beginning of the desorption test was in reality pseudo-isothermal before the powder sample temperature reached the desired value. However, the calibrated time interval within which the powder sample in the reactor reaches the furnace temperature is ~400–600 s in the 100–350 °C range, which is negligible compared to the desorption completion time especially at temperatures below 200 °C. Therefore, one can consider the test as being "isothermal" for any practical purposes at this range of temperatures. After desorption the powder without removal from the reactor was subjected to absorption at pre-selected temperature and pressure. The amount of desorbed/absorbed hydrogen was calculated from the ideal gas law as described in detail in [1]. Hydrogen desorption curves were also corrected for the hydrogen gas expansion due to the increase in temperature. The amount of desorbed/absorbed H_2 expressed in wt.% is calculated with respect to a total weight of powder including the additives.

Equilibrium plateau pressures at three different temperatures of 275, 285, and 295 °C were obtained in our Sieverts-type apparatus by a step-wise method by increasing pressure at a constant temperature until equilibrium was established. The enthalpy change of reaction (1) was estimated from the Van't Hoff equation [1]:

$$\ln\left(\frac{P_{H2}}{P_0}\right) = \frac{\Delta H}{RT} - \frac{\Delta S}{R} \tag{5}$$

where P_{H2} and P_0 is the equilibrium plateau pressure and atmospheric pressure, respectively, and ΔH and ΔS are the enthalpy and entropy changes of the hydriding/dehydriding reaction, respectively, T is the absolute temperature and R is the gas constant.

The apparent activation energy for desorption process was estimated from the obtained volumetric desorption curves at corresponding temperatures using the Arrhenius plot of k values with temperature [1]:

$$k = k_o e^{-E_A/RT} \tag{6}$$

where E_A is the activation energy, R is the gas constant and T is the temperature. The rate constant k was determined using the Johnson–Mehl–Avrami–Kolmogorov (JMAK) equation [1]:

$$\alpha = 1 - e^{-(k\cdot t)^\eta} \tag{7}$$

where η is the reaction exponent (the Avrami exponent) related to the transformation mechanism, taken as a free value characteristic for each individual temperature [1,16] rather than a fixed value for all temperatures, and α is the desorption fraction at time t.

3. Results and discussion

3.1. Morphology and microstructure of powder mixtures after milling for 25 h

Fig. 1a shows the backscattered electron (BSE) micrograph of the (($LiNH_2$ + 1.2LiH) + 5 wt.% G) mixture after ball milling for 25 h. The SEM micrograph of the morphology of the ($LiNH_2$ + 1.2LiH) mixture has already been shown in [12] and is not reproduced here. We did not estimate the specific surface area (SSA) in the present work because it was already estimated in [12]. The specific surface area (SSA) of the powder with the molar ratio 1:1 ($LiNH_2$:LiH) milled for 25 h was 59.6 m^2/g [12]. There is no reason to believe that the present powder would have a greatly different SSA after the same milling duration (25 h).

Fig. 1b shows the XRD patterns for (($LiNH_2$ + 1.2LiH)(pattern 1) and (($LiNH_2$ + 1.2LiH) + 5 wt.% G) (pattern 2) after ball milling. The principal diffraction peaks in both patterns belong to both $LiNH_2$ and LiH. Interestingly, there is no graphite peak present in the pattern 2 which strongly suggests that graphite transformed into an amorphous form as a result of a high energy ball milling. It is also interesting to note that both the LiOH and Li_2O diffraction peaks are observed in the mixture without graphite (pattern 1) whereas only the Li_2O peaks are observed in the mixture doped with 5 wt.% G (pattern 2). Possible direct reaction routes which can result in the formation of LiOH were suggested when LiH is exposed to air at room temperature [17]:

$$LiH + H_2O = LiOH + H_2 \quad \Delta G = -133.01\,kJ/mol \tag{8}$$

$$LiH + (1/2)O_2 = LiOH \quad \Delta G = -370.24\,kJ/mol \tag{9}$$

The absence of the LiOH peaks in the diffraction pattern 2 in Fig. 1b for the mixture with 5 wt.% G as opposed to the pattern 1 without G is a clear evidence that the graphite additive indeed formed a hydrophobic coating around the LiH particles preventing the occurrence of reactions (8) and (9) in the mixture with graphite.

The origin of Li_2O can be twofold. First, it can be present as a pre-existing impurity in commercial $LiNH_2$ and then it can also lead to the formation of LiOH in the mixture without graphite according to the following reaction [17]:

$$Li_2O + H_2O = 2LiOH\ \Delta G = -78.06\,kJ/mol \tag{10}$$

Second, Li_2O can also be formed at room temperature if there is a small amount of moisture present in the atmosphere according to the following reaction [17]:

$$LiH + (1/2)H_2O = (1/2)Li_2O + H_2 \quad \Delta G = -93.98\,kJ/mol \tag{11}$$

$$LiH + (1/4)O_2 = (1/2)Li_2O + (1/2)H_2 \quad \Delta G = -212.59\,kJ/mol \tag{12}$$

We did not estimate the grain size of the principal phases in the present work because it was already estimated in [12]. It was found in [12] from the corresponding XRD peak profile breadths that in the mixture ($LiNH_2$ + LiH) (1:1) after 25 h of ball milling (IMP68 mode) the grain (crystallite) size of $LiNH_2$ and LiH was 23 and 14 nm, respectively, with corresponding lattice strain of 4.62×10^{-3} and 0, respectively. One can reasonably assume that the grain size would be very similar after 25 h of milling in the present mixture ($LiNH_2$ + 1.2LiH) without and with 5 wt.% G additive.

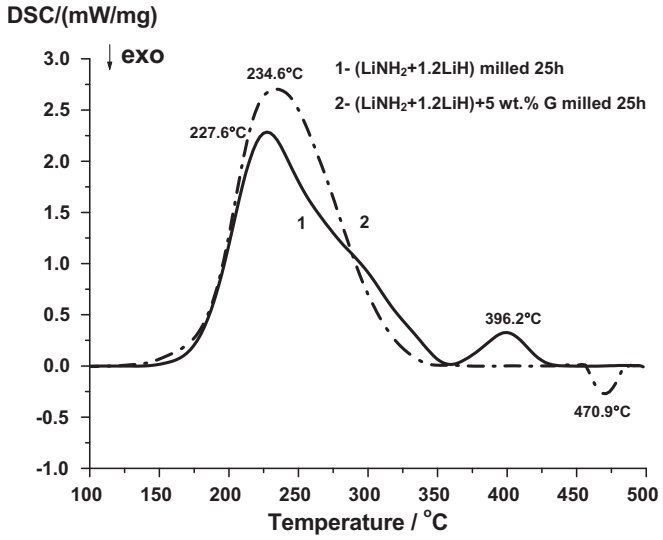

Fig. 2. DSC curves at a heating rate of 10 °C/min for the ($LiNH_2$ + 1.2LiH) mixture without and with 5 wt.% graphite both ball milled for 25 h.

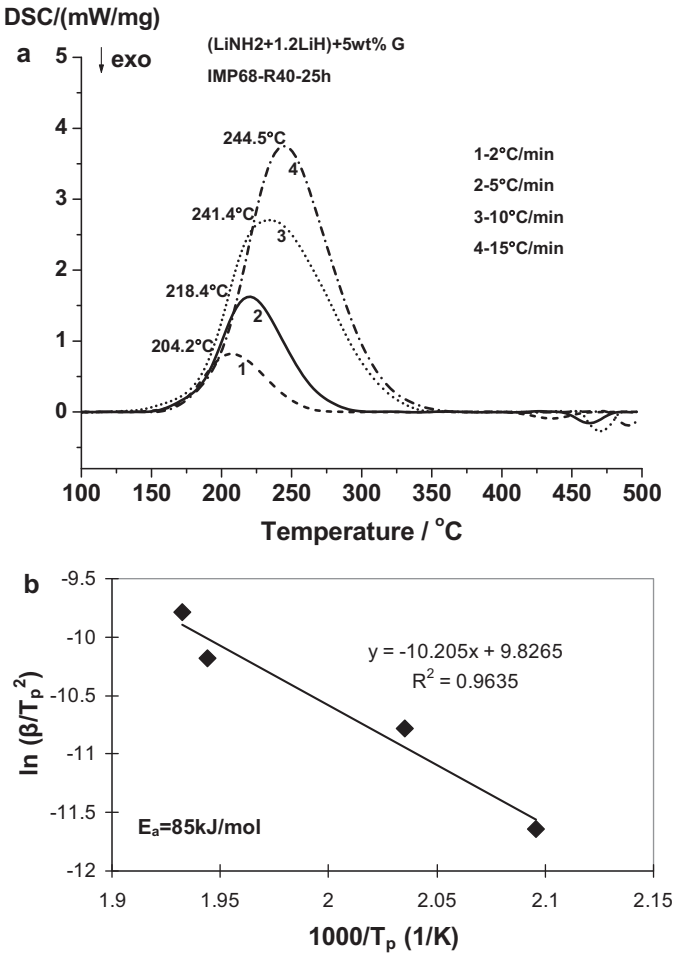

Fig. 3. (a) DSC curves at various heating rates and (b) the Kissinger plot for the apparent activation energy of dehydrogenation (reaction (1)) for milled (($LiNH_2$ + 1.2 LiH) + 5 wt.% G).

3.2. Thermal (DSC) behavior

Fig. 2 represents the comparison of the DSC profiles of ($LiNH_2$ + 1.2LiH) and (($LiNH_2$ + 1.2LiH) + 5 wt.% G) milled for 25 h. It

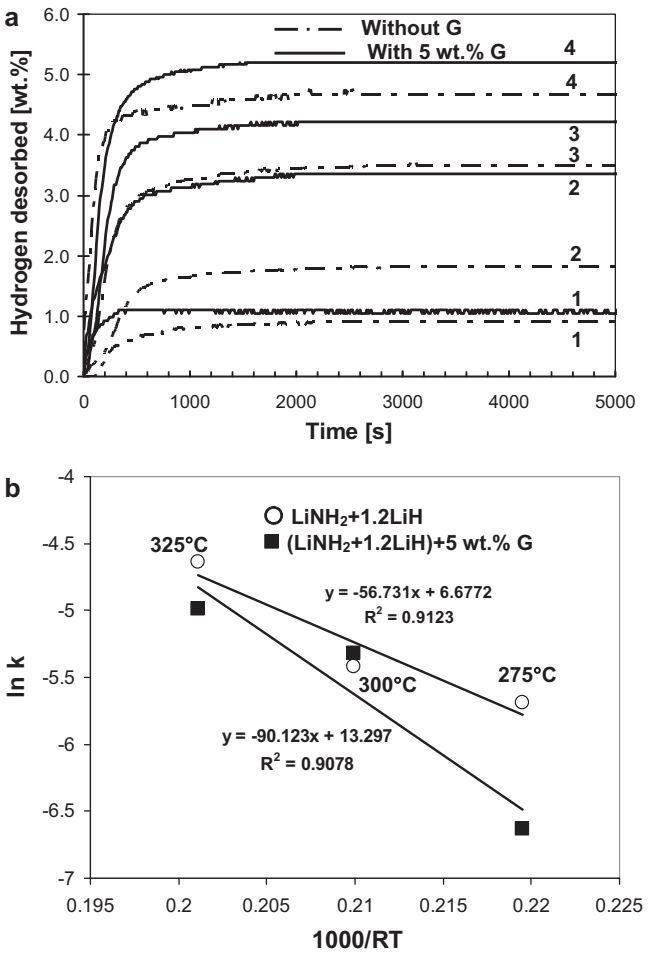

Fig. 4. (a) Desorption curves under 1 bar H_2 pressure (atmospheric) for 25 h milled ($LiNH_2$ + 1.2 LiH) and (($LiNH_2$ + 1.2 LiH) + 5 wt.% G) ((1) 250 °C, (2) 275 °C, (3) 300 °C, (4) 325 °C), and (b) Arrhenius plots for the estimate of the apparent activation energy for the mixtures without and with 5 wt.% G.

is very interesting that the mixture without graphite shows two endothermic peaks, a large and a small one, whereas the mixture with graphite shows one large endothermic and one small exothermic peak. In the case of ($LiNH_2$ + 1.2LiH) the first endothermic peak at 234.6 °C is related to reaction (1) in which hydrogen is being released and the second endothermic peak at 396.2 °C is due to the melting of retained $LiNH_2$ in the mixture and desorption of some NH_3 (reaction (2)). This retained $LiNH_2$ occurs due to the partial oxidation/hydrolysis of LiH which renders reaction (1) incomplete. For the mixture (($LiNH_2$ + 1.2LiH) + 5 wt.% graphite) the second endothermic peak disappears, indicating that graphite can prevent or at least substantially reduce the oxidation/hydrolysis of LiH. The hydrophobic synthetic graphite covers the surface of LiH and $LiNH_2$ such that water can be repelled from the surface. Therefore, a hydrolysis/oxidation of LiH can be prevented. The small exothermic peak at 470.9 °C for (($LiNH_2$ + 1.2LiH) + 5 wt.% G) is related to the oxidation of graphite.

The measurements of the apparent activation energy of hydrogen desorption according to the reaction (1) was conducted using two complimentary methods; the Kissinger (Eq. (4)) and the JMAK-Arrhenius (Eqs. (6) and (7)) method. Fig. 3a shows the effect of varying heating rate on DSC profiles which is an underlying principle of the Kissinger method for the milled (($LiNH_2$ + 1.2LiH) + 5 wt.% G) system. The corresponding Kissinger plot is shown in Fig. 3b. One should pay attention to the excellent correlation coefficients, R^2, obtained for the Kissinger plots in Fig. 3b which attest to the

accuracy of the method. The apparent activation energy of the mixture with 5 wt.% graphite is 84.9 kJ/mol. Considering the previously reported apparent activation energy of ($LiNH_2$ + 1.2LiH) which was 57.5 kJ/mol [12], the apparent activation energy of the mixture with 5 wt.% graphite becomes slightly higher. This behavior can be explained by the fact that the surfaces of $LiNH_2$ and LiH are covered with graphite. Generally, surfaces of the particles after ball milling become very reactive and are in an intimate contact with other reactants, so the apparent activation energy can be reduced. However, if these surfaces are coated with an inactive material like graphite, they can become less reactive and, additionally, the diffusion path and distance can be changed. Therefore, it seems from the results obtained for the apparent activation energy that graphite can hinder the surface reaction between $LiNH_2$ and LiH increasing activation energy.

3.3. Isothermal hydrogen storage behavior

Fig. 4a shows desorption curves of ($LiNH_2$ + 1.2LiH) without and with 5 wt.% G milled for 25 h, taken at various temperatures under 1 bar H_2 pressure. As can be seen, at temperatures of 275 °C, 300 °C and 325 °C desorption curves for the mixtures with graphite always show higher hydrogen capacity than the same mixtures without graphite. The only exception is the curve at 250 °C which shows a very low capacity of H_2 desorbed at this temperature (~1 wt.%). This striking capacity difference between the undoped and graphite doped mixture is most likely related to the fact that LiH in the mixture without graphite is partially hydrolyzed/oxidized. Therefore, $LiNH_2$ does not completely react with LiH and a hydrogen capacity is lost. As shown in Table 1, the mixture with graphite shows nearly theoretical hydrogen capacity if the purity of the starting materials is considered. This is one more piece of evidence pointing towards a very beneficial

Table 1
The calculated and experimental amount of H_2 desorbed from the 1:1.2 molar mixture ($LiNH_2$ + LiH) without and with 5 wt.% graphite (G) milled for 25 h.

	Theoretical capacity (wt.% H_2)		Experimental capacity (wt.% H_2) measured at 325 °C
	Purity of starting materials (%)		
	100	95	
$LiNH_2$ + 1.2LiH	6.2	5.9	4.7
($LiNH_2$ + 1.2LiH) + 5 wt.% G	5.9	5.6	5.2

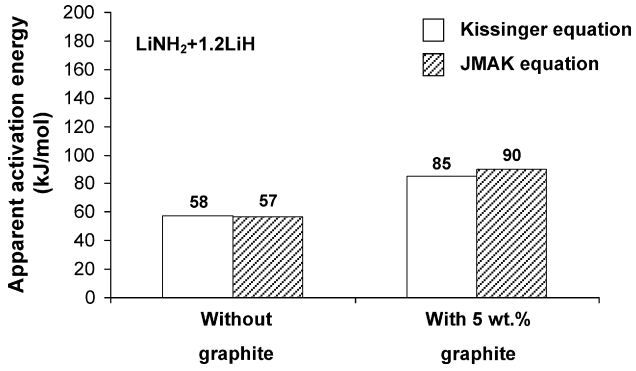

Fig. 5. Comparison of apparent activation energies obtained from the Kissinger and JMAK/Arrhenius methods for the mixtures without and with 5 wt.% G.

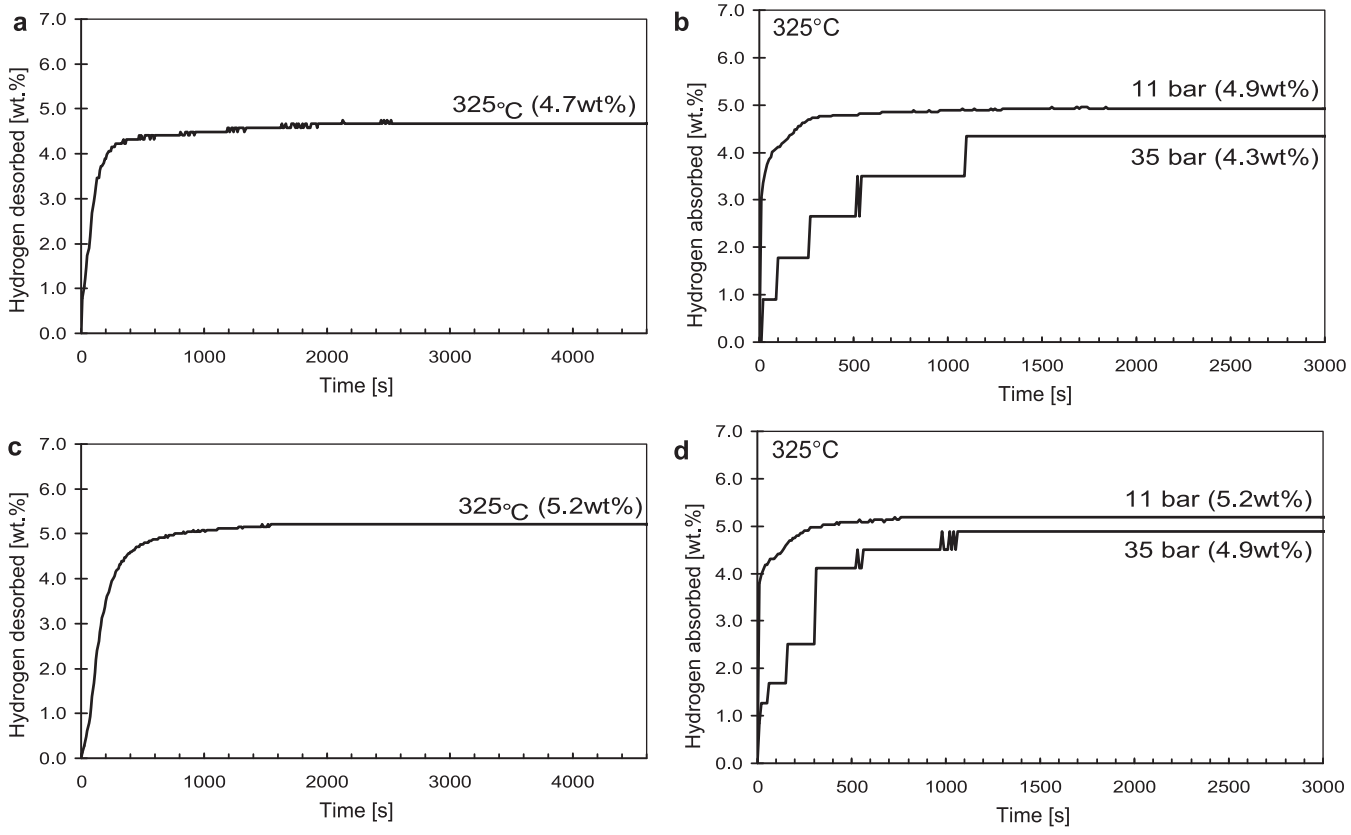

Fig. 6. (a) Desorption curve at 325 °C under 1 bar H_2 pressure and (b) corresponding absorption curves at 325 °C under 11 and 35 bar H_2 pressure for the ($LiNH_2$ + 1.2LiH) mixture ball milled for 25 h. (c) Desorption curve at 325 °C under 1 bar H_2 pressure and (d) corresponding absorption curves at 325 °C under 11 and 35 bar H_2 pressure for the (($LiNH_2$ + 1.2LiH) + 5 wt.% G) mixture ball milled for 25 h.

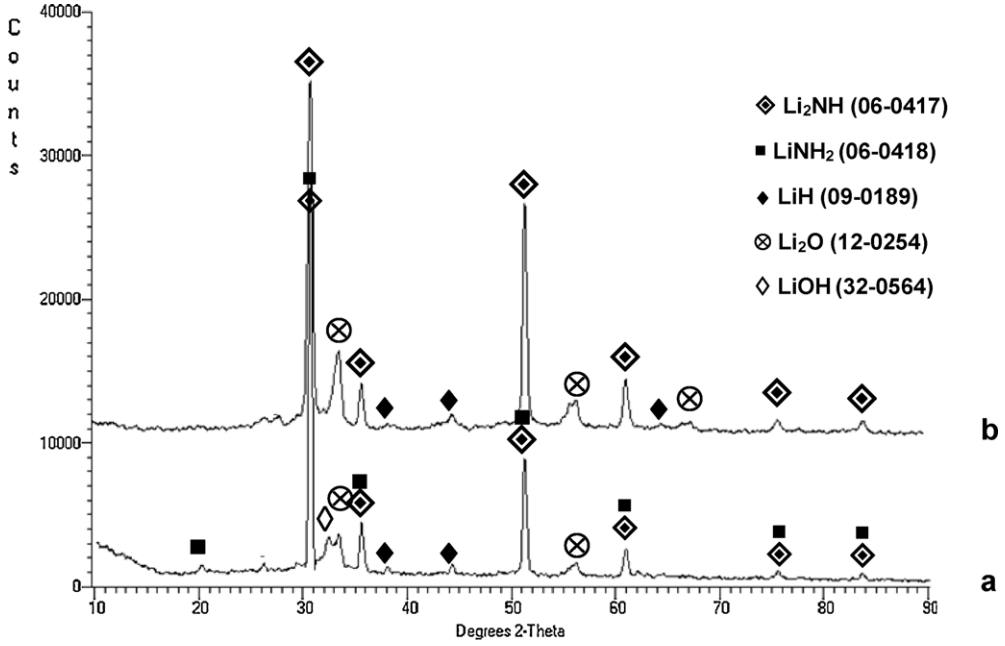

Fig. 7. Comparison of XRD profiles for (a) ($LiNH_2$ + 1.2LiH) and (b) (($LiNH_2$ + 1.2LiH) + 5 wt.% G) ball milled for 25 h and subsequently desorbed at 325 °C under 1 bar H_2 pressure.

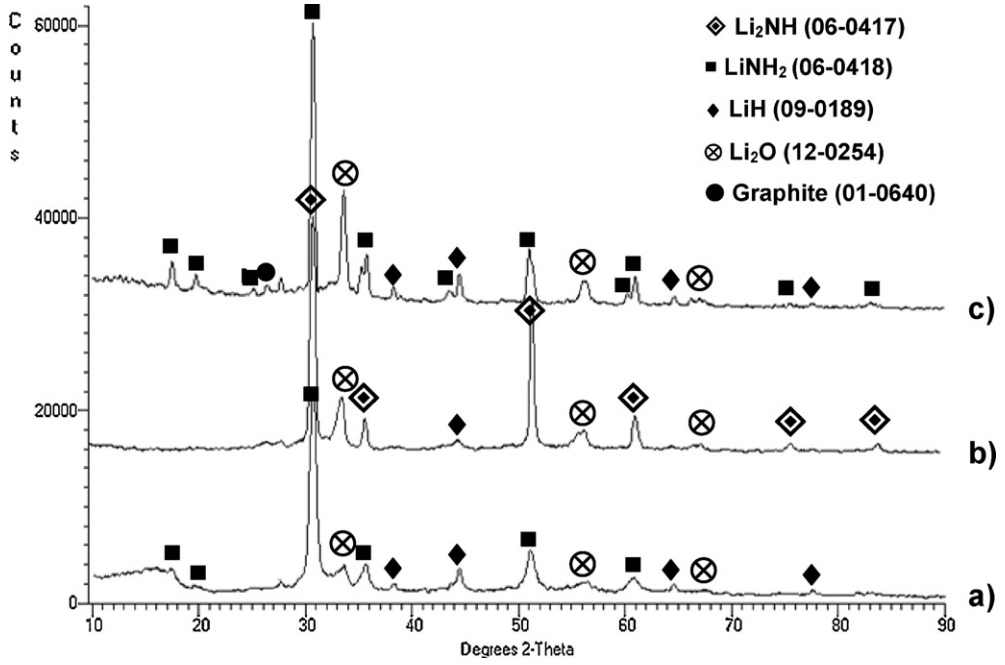

Fig. 8. Comparison of XRD profiles for (a) ball milled (($LiNH_2$ + 1.2LiH) + 5 wt.% G), (b) desorbed at 325 °C under 1 bar H_2 pressure after ball milling, and (c) absorbed at 325 °C under 11 bar H_2 pressure after desorption.

effect of the graphite additive. Fig. 4b shows the Arrhenius plots for the estimate of the apparent activation energy. The different slopes of the Arrhenius lines indicate quite a substantial difference in the apparent activation energies for the material with and without graphite. It is again clear that the addition of graphite actually increases the apparent activation energy from ~57 to ~90 kJ/mol.

Fig. 5 shows the comparison of the apparent activation energies obtained by the JMAK/Arrhenius and Kissinger method. The values of the apparent activation energies for the ($LiNH_2$ + 1.2Li) system without graphite were taken from [12] for comparison. It is obvious that both the Kissinger and volumetric method gives nearly identical values of the apparent activation energy of desorption according to Eq. (1).

Fig. 6a and c shows desorption curve for the undoped and 5 wt.% G doped mixture, respectively. Fig. 6b and d represents absorption curves at 325 °C under two different hydrogen pressures of 11 and 35 bar for the mixtures with and without graphite, respectively. Absorption behavior is quite similar irrespective of the presence of graphite. Interestingly, a lower absorption hydrogen pressure of 11 bars improves the kinetics of hydrogen absorption compared to a higher hydrogen pressure of 35 bars. Possibly, the high pressure hydrogen reacts at a high rate with the Li_2NH particle and subsequently a layer of $LiNH_2$ is immediately created on the particle

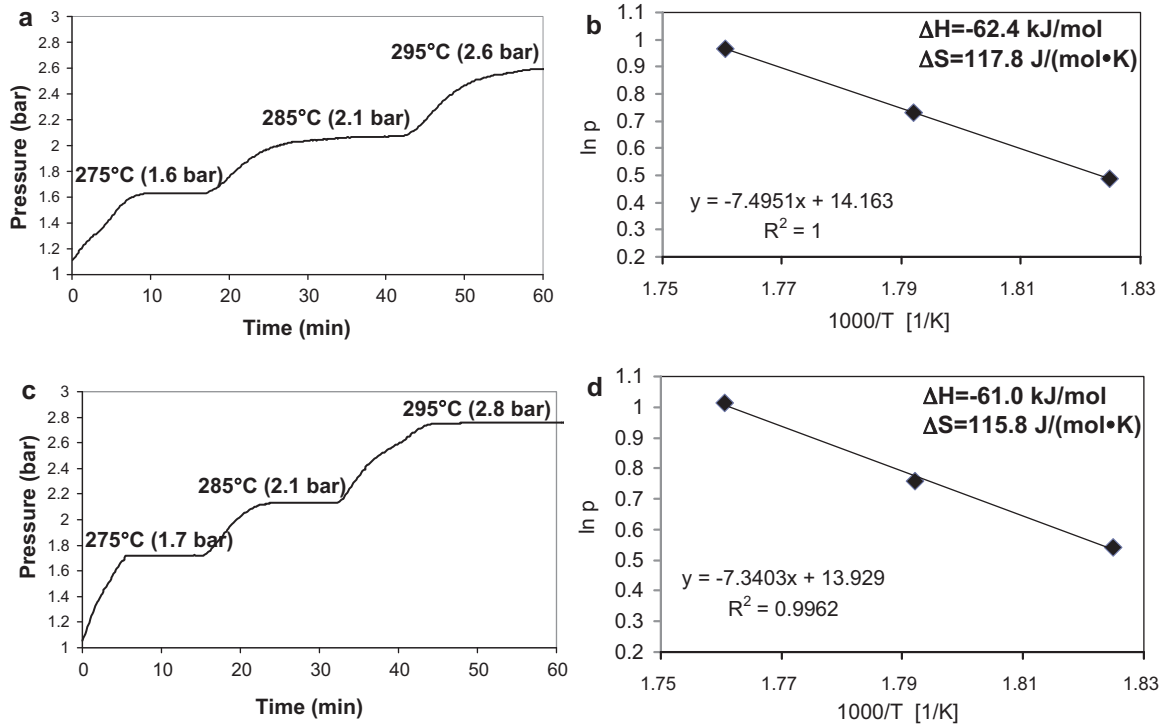

Fig. 9. (a) Step-wise PCT curves at varying temperatures and (b) corresponding Van't Hoff plot for the ($LiNH_2$ + 1.2LiH) mixture without graphite, (b) step-wise PCT curve at varying temperatures and (c) corresponding Van't Hoff plot for the ($LiNH_2$ + 1.2LiH) mixture with 5 wt.% graphite.

surface. This layer blocks the hydrogen from diffusing into the particle core which makes the absorption kinetics slower than those when using lower hydrogen pressure (11 bars).

Fig. 7 shows the comparison of XRD patterns of the mixtures with and without graphite after desorption test at 325 °C. According to the JCPDS file No. 06-0418 and 06-0417 for $LiNH_2$ and Li_2NH, respectively, most of the principal diffraction peaks of $LiNH_2$ and Li_2NH superimpose, except a couple of peaks at $2\theta = 17.7^\circ$ and 19.7° for $LiNH_2$, so these peaks can be taken as the indicators of the presence of the $LiNH_2$ phase in the mixture. It is noticeable that ($LiNH_2$ + 1.2LiH) without graphite still exhibits the $LiNH_2$ peak at $2\theta = 19.7^\circ$ (Fig. 7a), whereas, (($LiNH_2$ + 1.2LiH) + 5 wt.% G) does not exhibit any retained $LiNH_2$ peaks. The existence of $LiNH_2$ after desorption process is an indicator of incomplete desorption reactions (1)–(3). As proposed earlier [12], $LiNH_2$ is unable to completely react with LiH due to the partial hydrolysis and oxidation of LiH according to reactions (8), (9), (11) and (12) which make LiH inactive and consequently the unreacted $LiNH_2$ retains after the desorption process as evidenced by its diffraction peaks in Fig. 7a. This is additional strong piece of evidence that graphite can improve the stability of LiH because the XRD profile of ($LiNH_2$ + 1.2LiH) with graphite in Fig. 7b does not show retained $LiNH_2$ peaks after desorption. However, both mixtures still have LiH peaks after the desorption test. The LiH diffraction peaks in Fig. 7a, for the graphite-free ($LiNH_2$ + 1.2LiH) mixture, arise from the inactive LiH portion due to its hydrolysis/oxidation. In contrast, the LiH diffraction peaks after the desorption test of the (($LiNH_2$ + 1.2LiH) + 5 wt.% G) mixture in Fig. 7b arise from the unreacted excessive 20% mole LiH added to the mixture with graphite (molar ratio 1:1.2).

It must also be pointed out that at higher temperatures of desorption the conversion of LiOH into Li_2O may occur according to reactions (13) and (14) [18]:

$$LiOH + LiH = Li_2O + H_2 \quad \Delta G = -49\,kJ/mol \tag{13}$$

$$2LiOH = Li_2O + H_2O \quad \Delta G = 97\,kJ/mol \tag{14}$$

Li_2O formed at high temperatures may react with water and finally LiOH may be formed again at room temperature (after cooling) according to reaction (10). This mechanism is plausible for the ($LiNH_2$ + 1.2LiH) mixture (Fig. 7a) but it is not feasible for the ($LiNH_2$ + 1.2LiH) + 5 wt.% G) mixture (Fig. 7b) because in the latter Li_2O cannot react with water since it can be repelled from the hydrophobic graphite surface coating around the LiH particles. Therefore, most likely, the diffraction peaks of Li_2O observed in Fig. 7b arise from Li_2O which is already an impurity in commercial $LiNH_2$.

To confirm the reversibility of reaction (1), the XRD phase analysis for the mixture with graphite (($LiNH_2$ + 1.2LiH) + 5 wt.% G) after desorption and absorption at 325 °C under 11 bars was performed as shown in Fig. 8b and c in comparison to the XRD pattern of a ball milled sample in Fig. 8a. After dehydrogenation the $LiNH_2$ peaks disappear (Fig. 8b) and the Li_2NH peaks appear. The XRD pattern in Fig. 8c confirms that reaction (1) is totally reversible since after re-hydriding, the Li_2NH peaks disappear and the $LiNH_2$ peaks reappear again especially the peaks at $2\theta = 17.7^\circ$ and 19.7° which do not superimpose with the Li_2NH diffraction peaks.

3.4. Enthalpy and entropy change for a hydrogen desorption reaction

Some controversy in the literature related to the magnitude of the enthalpy change (ΔH) of the dehydrogenation reaction (−44.5 kJ/mol H_2 in [2] and −65.6 kJ/mol H_2 in [3]) prompted us to do the pressure–composition–temperature (PCT) experiments by a step-wise method (see Section 2). One must realize that in this method every following desorption is carried out on a partially desorbed sample containing less and less hydrogen. In addition, the increase in pressure occurs within a fixed time period during which some desorption may also occur. The method is much faster than the conventional PCT but simultaneously due to the factors mentioned above it may not be as accurate as the conventional PCT method.

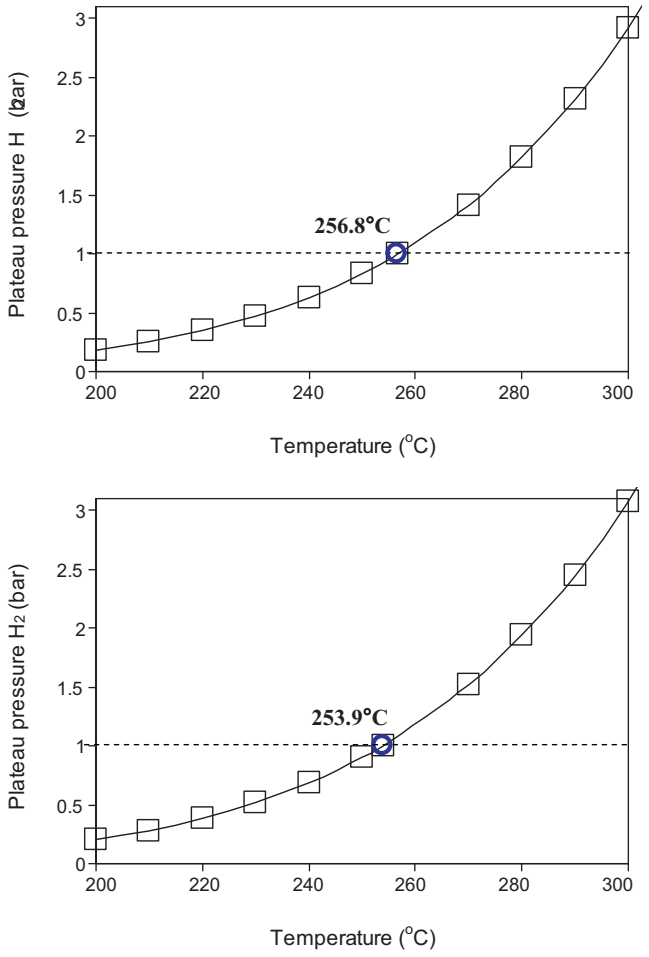

Fig. 10. Plateau pressure vs. temperature for (a) ($LiNH_2$ + 1.2LiH) and (b) ($LiNH_2$ + 1.2LiH) + 5 wt.%G mixture milled for 25 h.

Fig. 9a and c shows step-wise desorption curves at 275, 285 and 295 °C with corresponding equilibrium plateau pressures for undoped and 5 wt.% G doped mixtures, respectively. The results of the enthalpy and entropy change values obtained from the Van't Hoff relationship (Eq. (5)) are shown in Fig. 9b and d for the undoped and for the graphite-doped mixtures, respectively. As can be seen the enthalpy and entropy change of reaction (1) is −62.4 kJ/mol and −61.0 kJ/mol H_2 and 117.8 and 115.8 J/mol K for undoped and 5 wt.% G doped ($LiNH_2$ + 1.2LiH) system, respectively. Within an experimental error there is no measurable effect of graphite additive on the thermodynamic properties.

The values of the enthalpy change obtained in the present work are slightly lower than the one reported in [3] (−65.6 kJ/mol H_2). Excellent coefficients of the fit to the Van't Hoff lines in Fig. 9b and d give strong evidence that the step-wise method is, indeed, very accurate at least for the hydride systems investigated in the present work.

Fig. 10a and b shows the plateau pressure vs. temperature plots computed from the Van't Hoff relationship (Eq. (5)) and the thermodynamic data in Fig. 9b and d. As can be seen, the equilibrium temperature at atmospheric pressure of hydrogen (1 bar H_2) is 256.8 °C and 253.9 °C for the undoped and 5 wt.% G doped ($LiNH_2$ + 1.2 LiH) system ball milled for 25 h, respectively. Such high equilibrium temperatures also explain a very sluggish desorption rate at 250 °C as observed in Fig. 4a. It is also quite obvious that both of these hydride systems cannot be employed for hydrogen desorption/absorption below 100 °C as required by the DOE targets for the automotive hydrogen storage materials [19]. However, the easily reversible (($LiNH_2$ + 1.2 LiH) + 5 wt.% G) hydride system can be a potential candidate for hydrogen storage at higher temperatures, as related to high temperature fuel cells (e.g. solid oxide).

4. Conclusions

(1) After ball milling for 25 h the graphite (G) additive in the (($LiNH_2$ + 1.2LiH) + 5 wt.% G) mixture becomes amorphous.
(2) DSC analysis shows that for the mixture (($LiNH_2$ + 1.2LiH) + 5 wt.% G) the graphite additive can prevent the oxidation/hydrolysis of LiH since no melting peak of retained $LiNH_2$ is observed.
(3) Both the DSC and Sieverts-type test show that the addition of graphite increases the apparent activation energy of desorption from the ∼57–58 to ∼85–90 kJ/mol range.
(4) The Sieverts-type tests show that the graphite additive increases measurably the desorbed/absorbed capacity of hydrogen at 275 °C, 300 °C and 325 °C.
(5) The Sieverts-type tests show that the (($LiNH_2$ + 1.2LiH) + 5 wt.% G) system is fully reversible desorbing/absorbing ∼5 wt.% H_2 at 325 °C in the following reaction: ($LiNH_2$ + LiH ↔ Li_2NH + H_2).
(6) Step-wise PCT tests show that the enthalpy and entropy change of this reversible reaction is −62.4 kJ/mol and −61.0 kJ/mol H_2 and 117.8 and 115.8 J/mol K for undoped and 5 wt.% G doped ($LiNH_2$ + 1.2LiH) system, respectively. Within an experimental error there is no measurable effect of graphite additive on the thermodynamic properties.
(7) The Van't Hoff analysis of the obtained thermodynamic data shows that the equilibrium temperature at atmospheric pressure of hydrogen (1 bar H_2) is 256.8 °C and 253.9 °C for the undoped and 5 wt.% G doped ($LiNH_2$ + 1.2 LiH) system ball milled for 25 h, respectively. Such high equilibrium temperatures render it quite obvious that both of these hydride systems cannot be employed for hydrogen desorption/absorption below 100 °C as required by the DOE targets for the automotive hydrogen storage materials

Acknowledgements

This research was supported by the NSERC Hydrogen Canada (H2CAN) Strategic Research Network and NSERC Discovery grants which are gratefully acknowledged. The authors are grateful to Prof. Linda Nazar from the Department of Chemistry, University of Waterloo, for the usage of XRD equipment.

References

[1] R.A. Varin, T. Czujko, Z.S. Wronski, Nanomaterials for Solid State Hydrogen Storage, Springer Science+Business Media, New York, NY, 2009.
[2] P. Chen, Z. Xing, J. Luo, J. Lin, K.L. Tan, Nature 420 (2002) 302–304.
[3] Y. Kojima, Y. Kawai, J. Alloys Compd. 395 (2005) 236–239.
[4] T. Ichikawa, S. Isobe, N. Hanada, H. Fujii, J. Alloys Compd. 365 (2004) 271–276.
[5] T. Markmaitree, R. Ren, L.L. Shaw, J. Phys. Chem. B 110 (2006) 20710–20718.
[6] J. Lu, Z.Z. Fang, H.Y. Sohn, Inorg. Chem. 45 (2006) 8749–8754.
[7] J.H. Yao, C. Shang, K.F. Aguey-Zinsou, Z.X. Guo, J. Alloys Compd. 432 (2007) 277–282.
[8] W.I.F. David, M.O. Jones, D.H. Gregory, C.M. Jewell, S.R. Johnson, A. Walton, P.P. Edward, J. Am. Chem. Soc. 129 (2007) 1594–1601.
[9] L.L. Shaw, R. Ren, T. Markmaitree, W. Osborn, J. Alloys Compd. 448 (2008) 263–271.
[10] Y.H. Hu, E. Ruckenstein, J. Phys. Chem. A 107 (2003) 9737–9739.
[11] S. Ikeda, N. Kuriyama, T. Kiyobayashi, Int. J. Hydrogen Energy 33 (2008) 6201–6204.
[12] R.A. Varin, M. Jang, M. Polanski, J. Alloys Compd. 491 (2010) 658–667.
[13] A. Calka, A.P. Radlinski, Mater. Sci. Eng. A 134 (1991) 1350–1353.
[14] Patents: WO9104810, US5383615, CA2066740, EP0494899, AU643949.

[15] A. Calka, R.A. Varin, Application of controlled ball milling in materials processing, in: T.S. Srivatsan, R.A. Varin, M. Khor (Eds.), Proceedings of the International Symposium on Processing and Fabrication of Advanced Materials IX (PFAM IX), ASM International, Materials Park, OH, 2001, pp. 263–287.
[16] A. Calka, A.P. Radlinski, Mater. Sci. Eng. 97 (1988) 241–246.
[17] R. Ren, A.L. Ortiz, T. Markmaitree, X. Wan, J. Power Sources 177 (2008) 500–505.
[18] K.F. Augey-Zinsou, J. Yao, Z.X. Guo, J. Phys. Chem. B 111 (2007) 12531–12536.
[19] S. Dillich, DOE Hydrogen Program 2009 Annual Progress Report, IV.0 Hydrogen Storage Sub-Program Overview.